REPORT DOCUMENTATION PAGE

AFRL-SR-AR-TR-04-

0181

1. REPORT DATE *(DD-MM-YYYY)*	2. REPORT TYPE	3. DATES COVERED *(From - To)*
03/17/2004	Final	04/01/2001 - 06/30/2002

4. TITLE AND SUBTITLE
Integrated Vacuum Growth System for Hybrid Organic-Inorganic Materials

5a. CONTRACT NUMBER

5b. GRANT NUMBER
F49620-01-1-0248

5c. PROGRAM ELEMENT NUMBER

6. AUTHOR(S)
Prof. Vladimir Bulovic

5d. PROJECT NUMBER

5e. TASK NUMBER

5f. WORK UNIT NUMBER

7. PERFORMING ORGANIZATION NAME(S) AND ADDRESS(ES)

Research Laboratory of Electronics
Massachusetts Institute Of Technology
77 Massachusetts Avenue
Cambridge, MA 02139

8. PERFORMING ORGANIZATION REPORT NUMBER

9. SPONSORING / MONITORING AGENCY NAME(S) AND ADDRESS(ES)
Air Force Office of Scientific Research
4015 Wilson Boulevard
Arlington, VA 22203-1954

20040423 046

12. DISTRIBUTION / AVAILABILITY STATEMENT

Distribution Statement A: unlimited

13. SUPPLEMENTARY NOTES

14. ABSTRACT

Our recent demonstrations of efficient inorganic-quantum-dot light-emitting devices in molecular organic hosts indicate the vast potential of hybrid organic/inorganic nanostructured materials for development of practical active devices. Experience shows that essential to the high performance of such nano-structures is the high material purity and controlled device growth. Both can be improved through the use of the novel and versatile integrated materials deposition system developed in this program.

15. SUBJECT TERMS

16. SECURITY CLASSIFICATION OF:			17. LIMITATION OF ABSTRACT	18. NUMBER OF PAGES	19a. NAME OF RESPONSIBLE PERSON
a. REPORT	b. ABSTRACT	c. THIS PAGE			19b. TELEPHONE NUMBER *(include area code)*

Integrated Vacuum Growth System for Hybrid Organic-Inorganic Materials

Vladimir Bulović
Electrical Engineering and Computer Science Department
Massachusetts Institute of Technology
e: bulovic@mit.edu, t: 617-253-7012

Abstract

Our recent demonstrations of efficient inorganic-quantum-dot light-emitting devices in molecular organic hosts indicate the vast potential of hybrid organic/inorganic nanostructured materials for development of practical active devices. Experience shows that essential to the high performance of such nano-structures is the high material purity and controlled device growth. Both can be improved through the use of the novel and versatile integrated materials deposition system developed in this program.

Integrated Materials Growth and Analytical System

The integrated growth and analytical system provides a versatile environment capable of precise growth and testing of a variety of organic and inorganic materials in a thin-film form. These are used in fundamental studies on physical properties and processes of materials/structures or for development of novel organic/ inorganic device technologies.

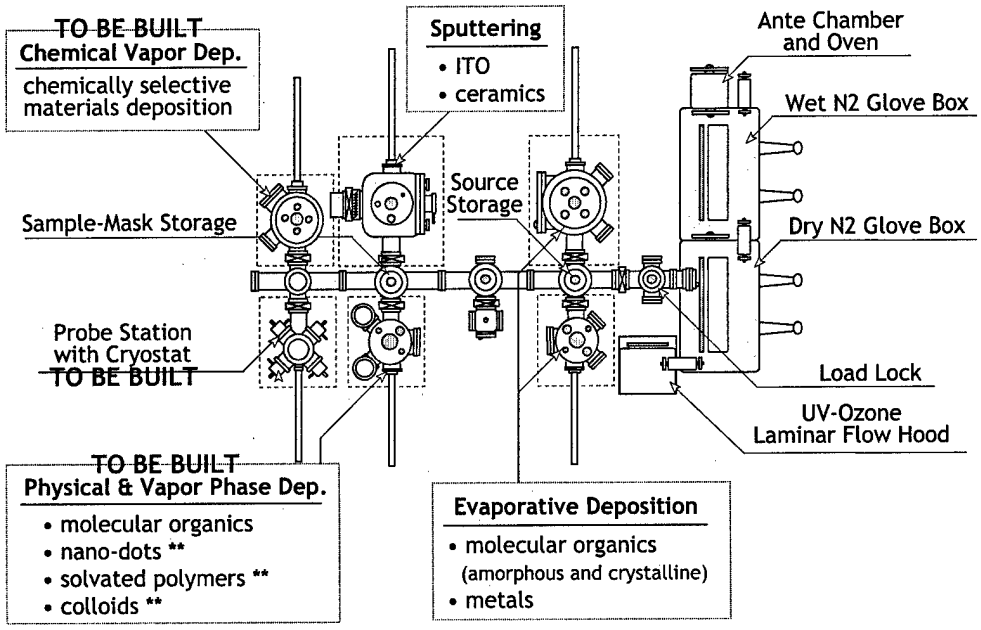

FIGURE 1 Integrated Materials Growth System. Both present and projected chambers are indicated. Projected chambers and chambers in construction are labeled as "TO BE BUILT". Materials sets that can be deposited with specific chambers are indicated.

Vacuum growth of organic and inorganic materials can generate atomically flat thin films of high purity, facilitating fabrication of complex multi-layer devices with excellent uniformity and sharp interfaces between adjacent layers. Such vacuum grown devices are highly reproducible from run to run, and can have complex structures containing thin layers of precisely controlled composition. Increased control over the growth parameter is essential for the better performance devices. Additionally, flexibility of van der Waal bonds in the organic thin films facilitate their integration with both conventional technologies and less conventional materials such as flexible, self-assembled, or conformable substrates.

FIGURE 2 Thermal Evaporator capable of co-deposition from six thermally heated sources.

Within this program we developed a versatile materials growth system (see Fig. 1) that combines conventional materials growth techniques with novel deposition methods developed in our laboratories. The completed growth system integrates the method for physical and vapor phase deposition of hybrid organic/inorganic thin-films with a low-pressure RF/DC sputtering chamber, an evaporative growth chamber (see Fig. 2), and a chemical vapor deposition chamber. The system is capable of depositing molecular organics, polymers, metals, metal oxides, inorganic nanodots, and colloids in a controlled layer-by-layer fashion. An in-situ shadow masking system enables fabrication of complex patterned structures inside a vacuum environment, while the integrated N_2-filled, dry glove box facilitates handling, measuring, and packaging of organic thin film samples that are susceptible to reactions with atmospheric oxygen and water vapor (see Fig. 3). The glove box system is divided into two sub-sections that have independent atmospheres. The left section connects the glove-box environment to the load-lock of the vacuum system. The right section has a built-in spin-coater enabling spin-depositon of materials such as inorganic quantum dots and polymers in an inert environment of the glove-box.

When the analysis chamber is built, the completed samples will be in-situ tested by contacting them with an electrical probe attached to an X-Y-Z manipulator. Optical ports on the analysis chamber allow for a telescopic view of the devices and facilitate optical excitation of probed samples. Optoelectronic properties of the hybrid materials and structures will be investigated at a range of temperatures form 5 K to 600 K, generated by

the liquid helium cryostat and the boron-nitride heater situated behind the sample stage. Existing chambers are presently connected to the central transfer system that has linear degrees of freedom. Maximum substrate size is 10 cm with a 5% variation in the thickness and composition of deposited films over the substrate area.

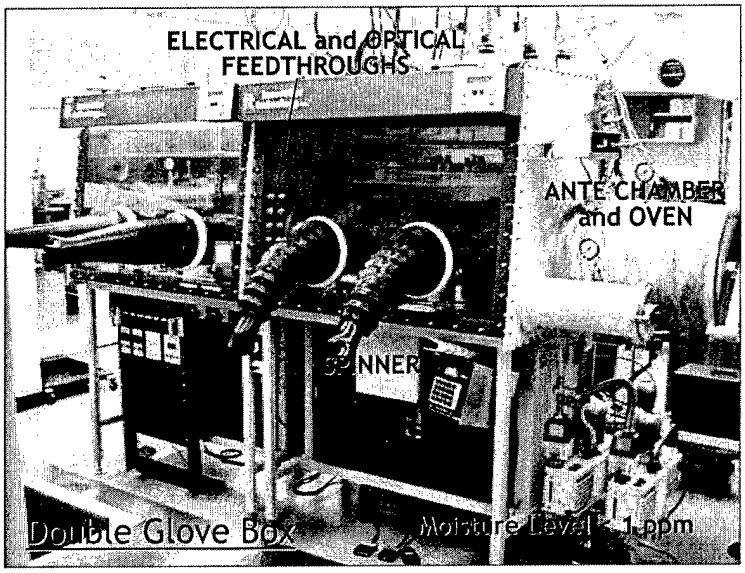

FIGURE 3 Glove Box system consisting of a vacuum-connected section (left) and an integrated spin-coater section (right). The two sections have independent atmospheres and are connected to each other via a pass-through chamber.

The integrated growth system is the centerpiece of our materials growth effort, as in its completed form it will accommodate solvent-free deposition and co-deposition of polymers, colloids, and molecular organic materials in vacuum. Its versatility is unsurpassed in the field of organic/inorganic materials deposition, and it is among the first to integrate organic and inorganic material deposition methods.

Typical base and operating pressures for individual chambers are listed in the table below.

SYSTEM	Base Pressure [Torr]	Operating Pressure [Torr]
Load Lock	10^{-7}	10^{-7} to atmosphere
Sputtering	10^{-9}	10^{-3} to 10^{-2}
Evaporative	10^{-10}	10^{-10}
Central Transfer	10^{-9}	10^{-7} to 10^{-9}

Central Transfer System

Constraints on the design of our linear transfer system are typical of the custom design work done in designing of the entire system. The compact transfer line was designed to fit in the elongated laboratory footprint, and is capable of integrating up to 8 different deposition systems. Its modular design enables further elongation of the transfer line by adding additional 3 foot-long line sections. Also, this system was designed for ease of use, and as fool-proof as possible, to maximize up time and minimize the skill level needed to be a user of the facility. As a result tolerances of up to 0.125" are allowed in misalignment of mating parts during transfer. The design of the transfer line and all of its

parts and components was done using the computer aided design tool Solidworks. Fig 4 shows two external views of the finished design as well as a photograph of the actual system installed in the lab. The difficult portion of the transfer line design is in the details. It allows transfer of substrates and shadow masks over distances of 13 feet, and yet the freedom of motion of any of the mating parts is at most 0.125 of one inch. This is so that there can be minimal strain on any given part, which will in turn minimize wear and bending of the precision machined parts. Two good examples of this precision are in the loadlock handoff and in the lateral fork handoff, drawings and pictures of which are shown in Fig. 5.

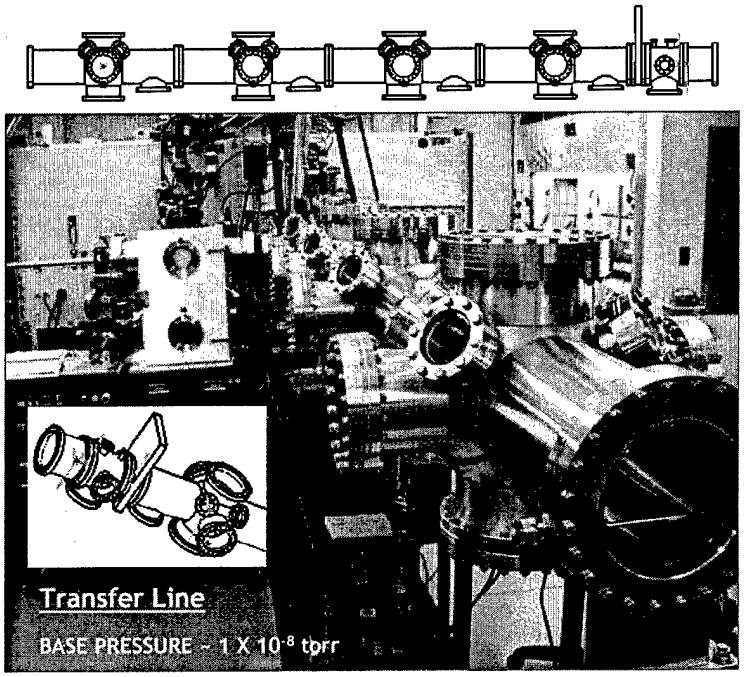

FIGURE 4 Photo of the 12' long linear transfer system with loadlock. (top and inset) Solidworks drawings of the transfer line in two orientations.

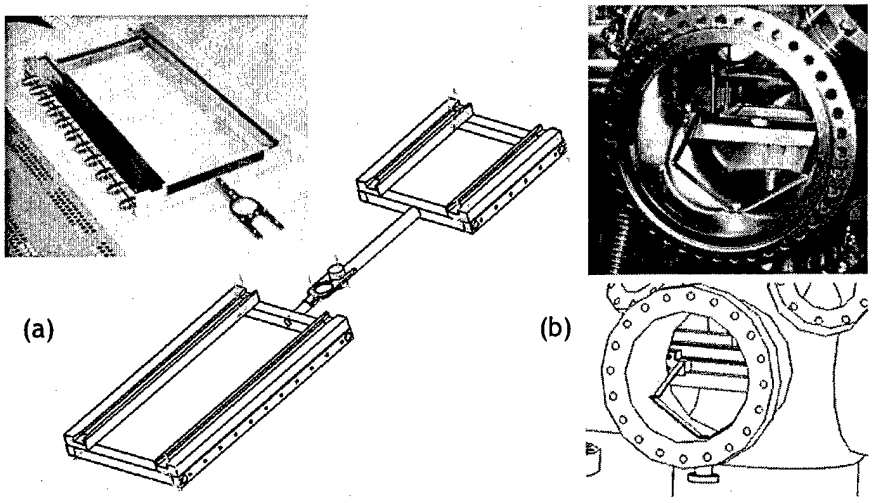

FIGURE 5 (a) Photograph of the caboose that rides the rails of the 13' chamber, and transports the substrate holders and shadow mask holders. Solidworks view of both the engine and the caboose in their "hand-off' configuration. (b) Photograph (and Solidworks perspective view) of the lateral alignment mechanics that ensure perfect insertion of the transfer fork into the

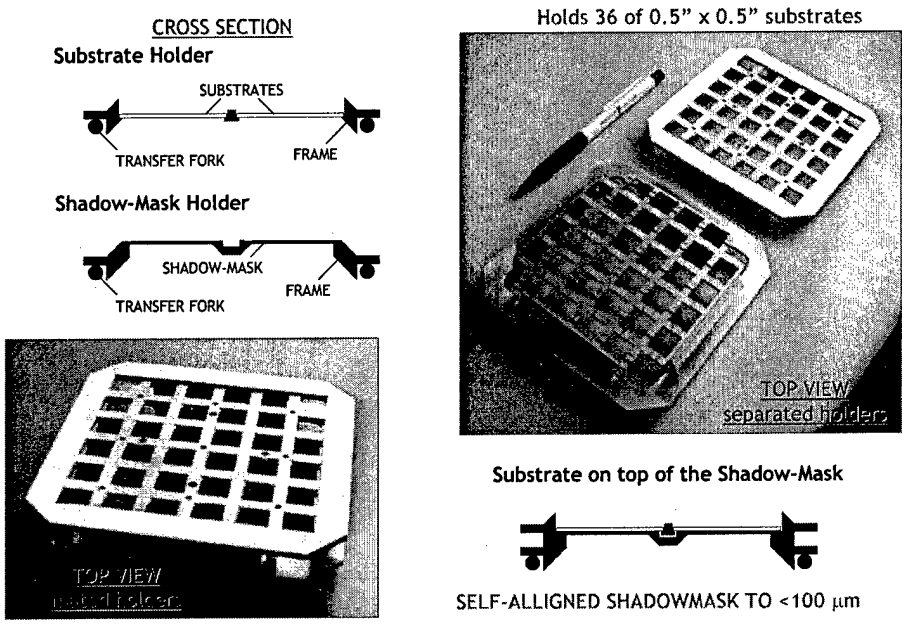

FIGURE 6 Sample holder and integrated, self-aligned shadow mask holder.

In-Situ Shadowmasking

The method of handling the typical fragile shadow masks within stainless steel vacuum chambers was a challenge in and of itself. Figure 6 shows our solution to this challenge. This two piece stack allows the separate handling and storage of shadow masks, which can then be self-aligned within ultra-high vacuum conditions to contact mask substrates loaded into the substrate holder. Alignment accuracy of the self-aligned shadowmasking process is estimated to be better than 100 μm. The substrate holder and the shadowmask is designed to accommodate ether 36 of 0.5" by 0.5" substrates, 9 of 1" by 1" substrates, 4 of 1.5" by 1.5" substrates, or a single 4" by 4" substrate.

Evaporative Deposition

Conventional evaporative deposition is a standard method for growth of molecular organic thin films. Our extensive experience with this growth technique indicates that its significant shortcoming is in the difficulty of fine control of the deposition rate. During a typical organic layer deposition it is common to observe growth rate variation of 10% or more. This is typically associated with uneven heating of the solid source material that undergoes sublimation during the deposition process. Fine control of deposition rates over extended period of time is most important during co-deposition of thick layers of two dissimilar materials, or when a graded doping profile is desired.

Our system is well suited for growth of precisely doped structures (Fig. 7). We are also developing a shuttering mechanism that will allow us to deposit programmable doping profile, such as graded doping concentration with the thickness of the deposited film, or doped multi-quantum well structures.

Additionally, the evaporative growth system has an integrated shadow-masking stage that allows for growth of several different samples during the same deposition run. The grown samples can vary in thickness, or alternatively doping concentration. This capability allows parallel growth of a large number of samples, yielding larger data sets and deeper insight into the examined phenomena.

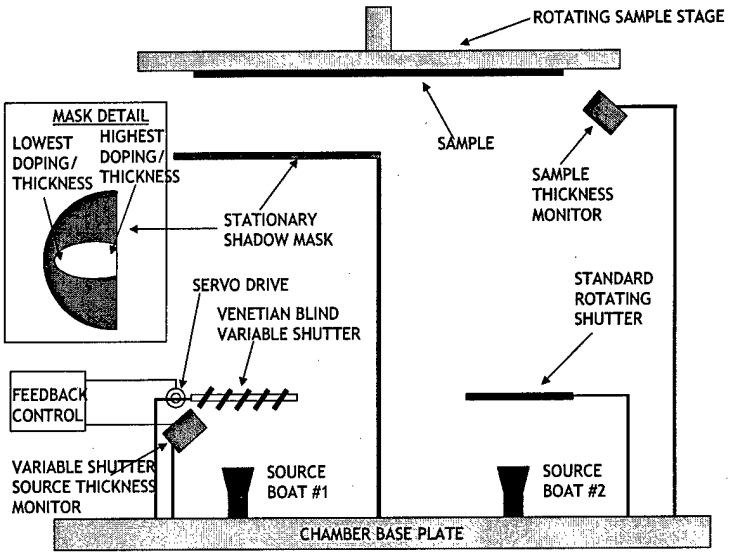

FIGURE 7 - Elements of the evaporative deposition chamber.

The system houses six thermally heated Molibdenum boats placed around the center of the chamber and tilted at 15° away from normal, aimed to provide maximum uniformity at the target area. The base is baffled to separate the sources into two groups of three cells, where each group shares a common electrode. A thickness monitor is placed at the level of the substrate to record the thickness of the deposited film. A second thickness monitor is placed in vicinity of the left bank of sources to monitor the source rate. The resistively heated boats can be operated in parallel, with up to two boats depositing at one time. The two thickness monitors allow for the flux of each component to be controlled individually. Baffles prevent cross-talk between boats. This feature is crucial for co-evaporation experiments.

The substrate holder is designed to accept sample pucks and shadow mask systems described above. The substrate holder can be moved up and down to assist in the loading/ unloading process, and rotates during deposition. To avoid inadvertent introduction of pumping stack oils into the chamber, we choose the pumping stack to be oil free consisting of the high-vacuum turbo pump and a low vacuum scroll pump backing the turbo and used in the initial chamber pump-down.

The substrates mounted onto the substrate holder (Fig. 6) enter the chamber from the linear transfer line using a magnetic transfer arm and are set into the rotating substrate holder. The system is then isolated from the vacuum line and the deposition is performed. A key feature of this arrangement is that samples can be moved from the evaporator to other equipment (e.g. a sputtering system) without breaking vacuum. Self-aligning shadow masks (Fig. 6) can also be exchanged on substrates in vacuum. The samples enter and exit the transfer line through a load lock that empties into a low oxygen and low moisture atmosphere glovebox.

Scientific and Technological Impact

The versatility of the proposed integrated system is unsurpassed in the field of organic materials deposition, and it is among the first to integrate organic and inorganic material deposition methods.

Development of active hybrid organic/inorganic-optoelectronics will lead to investigations of physical processes in hybrid materials such as exciton energy transfer, photogeneration, and charged carrier transport. These fundamental findings will have a direct impact on practical applications of hybrid solids in optoelectronic devices, influencing treatment of hybrid thin films, heterojunctions, multilayers, quantum wells, and nano-patterned organic/inorganic materials.

Example 1:
Inorganic Quantum Dots in Organic Host Matrices for Efficient LEDs

Using the integrated growth system, we recently demonstrated the first efficient hybrid organic/inorganic light emitting devices (LEDs), with saturated color emission, whose performance reaches that of the all-organic LED technology (Fig. 8) [Coe *et al.*, Nature 420, 800 (2002)]. The hybrid LEDs are large-area, efficient light emitters consisting of luminescent inorganic nanocrystals (quantum dots) embedded in organic LED structures. They represent a completely new technology platform for development of the flat-panel displays and the flat-panel lighting. Their greatest benefit is in the ease of tuning their saturated emission color across the visible spectrum (by changing the size of the nanocrystal), and in their potentially longer operating lifetimes as compared to the all-organic LEDs.

(a) CdSe Quantum Dots

Nanocrystal quantum dots (QDs) are semiconductor nanoparticles that are chemically synthesized using simple benchtop techniques. Their sizes can be precisely controlled in

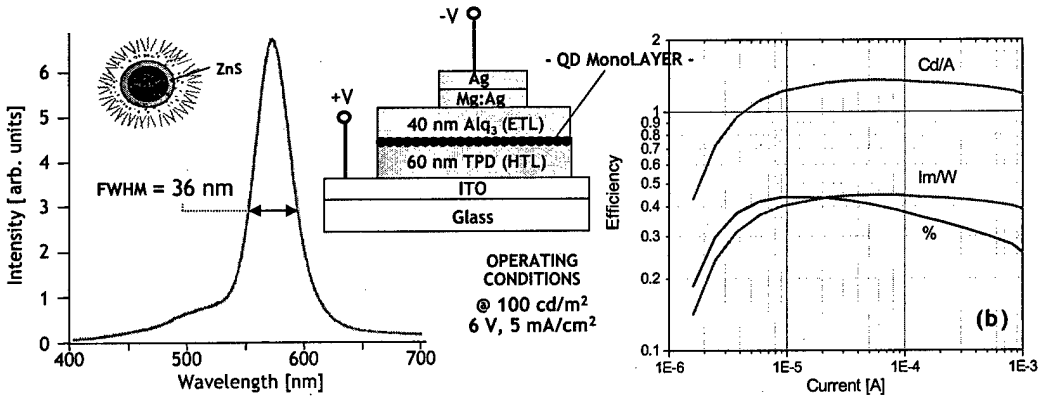

Figure 8- Hybrid organic/inorganic light emitting device contain inorganic QDs. (Inset) QD-LED cross section. (left) Electro-luminescence spectrum at ~100 cd/m^2, with inset device cross section. (right) QD-LED quantum efficiency in percent units, and luminescence efficiency in units of Cd/A and lm/W.

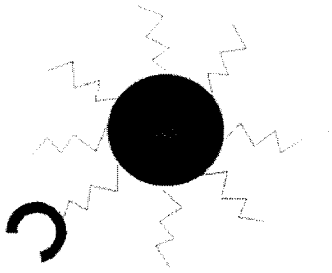

Figure 9 - Schematic of a QD showing an optically active core, a protective inorganic shell, an organic ligand shell, with one of the ligands functionalized.

a range from 1 to 10 nanometers. Electrons and holes are delocalized in QDs in states that are reminiscent of atomic wavefunctions. The energy of these states is strongly size-dependent: emission from CdSe QDs can be tuned across the entire visible spectrum by changing the size of the nanocrystals. Nanocrystal QDs can be synthesized with narrow size distributions so that the bandwidth of the emission can be < 30 nm. The dots are grown in organic solvents. Their surface is covered with a ligand shell that can be easily exchanged, giving the dots the potential for broad chemical and electronic flexibility (Fig. 9). The combination of broad spectral tunability and chemical flexibility make nanocrystal QDs ideal chromophores for opto-electronic applications in organic/inorganic hybrid structures such as QD-LEDs.

The quantum dot LEDs (QD-LEDs) incorporate CdSe nanocrystals in a molecular organic host via spin-on deposition of solvated materials. Spin-casting results in the formation of an organic/nanocrystal bilayer film due to the alkyl/phenyl phase segregation, where by alkyl-coated nanocrystals form a densely packed single monolayer on top of the conjugated organic film (see Fig. 10 and device cross section in Fig. 8). The devices are completed by thermally evaporating thin organic films and a metal cathode on top of the organic/nanocrystal layers. These first devices operate with a quantum efficiency of 0.4%, they have a saturated color, and brightness of 1500 cd/m^2 at current density of 120 mA/cm^2, corresponding to luminescence efficiency of 1.25 cd/A, as compared to the best previous results for nanocrystal-LEDs of 600 cd/m^2 at 1 A/cm^2, corresponding to 0.06 cd/A.

The remarkable 20-fold improvement in the electroluminescence efficiency of our QD-LEDs is attributed to the optimized device structures and improved photoluminescence

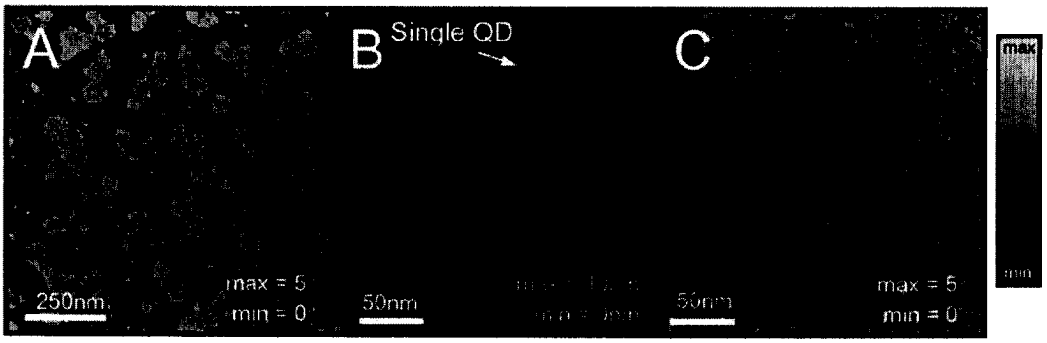

FIGURE 10 - AFM images showing the surface morphology of various organic/nanocrystal films. (A) Phase image of a partial monolayer of nanocrystals on top of organic thin film after phase segregation during spin-coating. Nanocrystal surface coverage is 21%. (B) Height image of a close-up of (A) showing both an island of nanocrystals as well as individual nanocrystals (QDs) on a flat organic background. (C) Phase image of a complete, hexagonally packed monolayer of nanocrystals phase segregated from the underlying organics. Grain boundaries between ordered domains of nanocrystals are observable.

efficiency and chemical stability of nanocrystals. The technologically innovative step of generating the self-assembled nanocrystal monolayer through phase segregation, allows us to position the nanocrystals in the recombination zone of the multilayer active organic EL device. Their confinement to the device active region maximizes the efficiency of nanocrystal usage. Furthermore, the use of alkane/phenyl phase segregation to create spin-cast heterostructures provides a new general method for the fabrication of organic or hybrid devices.

The fundamental limits of QD-LED performance are different than those of all organic LEDs. The discrete energy structure of QDs gives rise to a narrow emission spectrum , which in our electroluminesent devices is as small as 32 nm at full-width-half-maximum (FWHM). In contrast, molecular organic LEDs have a typical FWHM of between 50 and 100 nm. The vibrational structure of structurally flexible organics typically generates broad single molecule emission spectra at room temperature. The same is not true of the rigid, covalently bonded inorganic QD, for which single QD spectroscopy shows that the fundamental FWHM linewidth at room temperature is 14 nm with a symmetrical, gaussian shape. It is the combination of spectral diffusion and size distribution of QDs in a specific sample that yields further line broadening. However, it is reasonable to expect that current techniques in QD preparation and processing could yield QD-LED line widths that are as narrow as 25 nm, a feat that has already been accomplished in solution. Such true color saturation would benefit applications where efficient production of narrowband light is desired. In particular, the creation of high luminous efficiency red and blue LEDs requires both high external quantum efficiency as well as narrowband emission, to prevent the bulk of emission from occurring in the infrared or ultraviolet, respectively, where our eyes have minimal response.

With the demonstrated improvement in the luminescent power efficiency of QD-LEDs, we still have not reached the fundamental limits of device performance in both quantum efficiency and color saturation. We expect that with our development of the new

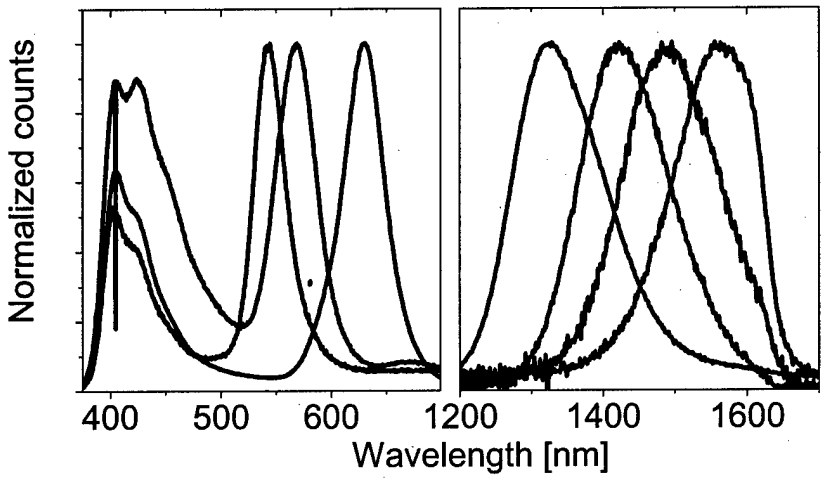

Figure 11 - Electroluminescence spectra from the visible to the near infrared of (left) CdSe and (right) PbSe based QD-LEDs.

methods for growth of QD-films in vacuum, higher material purity will be obtained. Performance of such vacuum-grown QD-LEDs could match and potentially exceed that of conventional organic thin-film LEDs, resulting in durable, integratable, highly-efficient light sources of nano-scale thickness. By changing the diameter of the CdSe core from 22 to 65Å, the peak luminescence wavelength can be precisely tuned from λ=470 nm to λ=640 nm with a typical spectral full width at half of maximum of less than 35nm. Fig. 11 shows the electroluminescence spectra of a series or visible and infra-red emitting QD-LEDs. Such broadly tunable, saturated color emission of quantum dots is unmatched by any class of organic chromophores. Furthermore, environmental stability of covalently bonded inorganic nanocrystals suggests that device lifetimes of hybrid-LEDs should match or exceed that of all-organic LEDs.

Example 2:
QD Monolayer Formation via Material Phase Segregation

QD-LEDs demonstrate that sheets of single QD monolayers, square centimeters in size, can be employed in electrically active devices. This minimizes QD material use to the active device region. The material phase segregation that governs formation of the organic/QD spin-cast thin film bilayers is a general and, we expect, widely applicable fabrication process. The process is governed by the physical size and chemical character of the two solvated constituents; the organic molecules in our devices are small (~1 nm) and have aromatic character, while the QDs are large in comparison (>3 nm) and present a surface that consists of mostly alkane chains. In general, phase segregation is not limited to aromatic/aliphatic pairs, but governs the interaction between any pair of materials with disparate chemical functionality. To date, the phase segregation phenomenon has been observed in spin cast solutions of (CdSe)ZnS core-shell/TOPO capped QDs and PbSe/oleic acid capped QDs with both α-NPD and TPD in chloroform and chlorobenzene.

Example 3:
Infra-Red QD-LEDs

Using the integrated growth system we also demonstrate large area (mm^2 in size) infrared electroluminescent devices using colloidally grown PbSe quantum dots (QDs) in organic host materials (Fig. 11). By changing the QD size the electroluminescence is tuned from 1.33 μm-1.56 μm with a full width at half maximum of <160 nm (< 0.11 eV). This represents only a portion of the accessible QD tuning range, as the lowest energy optical absorption peak of our PbSe solutions can be tuned from 1.1 eV (corresponding to wavelength λ = 1.1 μm and 2.6 nm diameter QDs) to 0.56 eV (λ = 2.2 μm, 9.5 nm diameter). Such large area emitters in the near infrared have been identified as technologically useful for chemical spectroscopy and sensing, night vision applications, and could be incorporated into an on-chip optoelectronic integrated circuit.

PbSe is a convenient choice for inorganic semiconductor QDs for NIR applications ($\lambda > 1$ μm), as the colloidal synthesis is reproducible and yields highly monodisperse nanocrystals. In addition, the exciton Bohr radius is large (46 nm), leading to strong confinement of QD excitons throughout the synthetically accessible range of 2 nm to >10 nm (corresponding to absorption peaks λ = 1.0 μm (1.2 eV) to >2.4 μm (<0.5 eV), respectively). Figure 12(a) shows typical absorption and emission spectra for 5.0±0.5 nm diameter PbSe QDs, while Fig. 12(b) depicts an ordered layer of 4.0±0.5 nm diameter QDs imaged by high resolution transmission electron microscopy, showing their highly crystalline structure in the inset.

The NIR EL spectrum of QD-LEDs closely resembles the PL spectrum of the corresponding QD solution (see Fig. 12(a)). The tunability of QD-LED emission as a function of the QD diameter is shown in Fig. 11(a), with EL spectral peaks at 1.33, 1.42, 1.50, and 1.56 μm. The FWHM of all four devices is <160 nm (< 0.11 eV). The devices also have an emission peak at 530 nm (not shown) due to exciton recombination within the Alq_3 ETL (or 405 nm corresponding to TPD EL when BCP is used as the ETL). We note that the InGaAs photodiode array used to record all of these spectra has low detection efficiency for λ >1.6 μm, modifying the apparent shape of the 1.56 μm emission peak.

The electrical characteristics of all the QD-LEDs of this study are similar, with a linear (J) versus voltage (V) dependence for V<3 V, and power law dependence, $J \propto V^9$, when light is emitted. This is consistent with the properties of an Alq_3/TPD device, though the operating voltage is a few volts higher, possibly due to QD charge trapping or interface dipole realignment. The PbSe QD-LED NIR external quantum efficiency is measured to be 0.001%, using a Silicon wafer to filter out visible emission from organic EL. The visible emission originates from Alq_3 and TPD and has an external EL quantum efficiency of 0.1-0.3%. These QD-LEDs demonstrate the feasibility of generating controllably tunable λ >1.3 μm EL in a large area device, and give us a starting point in the creation of higher efficiency devices in the spectral range of 1.2 μm < λ < 2.2 μm.

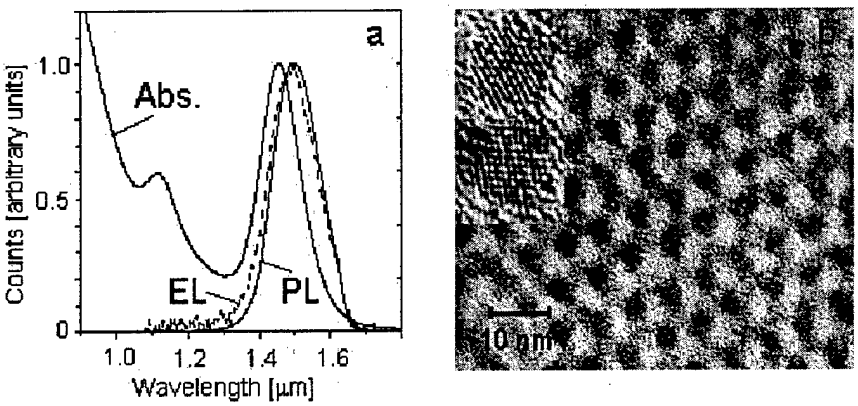

Figure 12 - (a) Typical absorption (peak at 1.456 μm), photoluminescence (peak at 1.500 μm), and electroluminescence spectra (peak at 1.495 μm) of 5.0±0.5 nm diameter PbSe particles; (b) HRTEM Image of 4.0±0.5 nm diameter PbSe particles with two enlarged images (inset).

Example 4:
Solid State Solvation

The integrated growth system facilitates our investigation of physical processes in organic materials. One example of this work is the solid state solvation for tuning the luminescence energy of organic chromophores.

Emission and absorption spectra of many organic dyes in liquid solutions depend on the local electric fields generated by the surrounding polar solvent molecules. This "solvation effect" is a result of intermolecular solute-solvent interaction forces (such as dipole-dipole or dipole-induced dipole) that tend to stretch molecular bonds and shift charge distribution on molecules, altering the energy difference between the ground and excited states of the solute.

The solvation effect is also present in molecular solids where closely packed polar molecules can generate large local electric fields. The first investigations of this effect show luminescence shifts in excess of 35 nm (changing emission form yellow to orange to red) for DCM2 laser dye doped in Alq_3 host matrix (see the picture of green to red luminescent slides in Fig. 13). Initial measurements of time resolved luminescence of polar luminescent dyes indicate that spectral shifts also take place during the luminescent process (see the Temporal Response plot in Fig. 13 that shows a typical contour trace of luminescence intensity as a function of wavelength and time for DCM dye in Alq_3). In the example shown most of the spectral shifting takes place during the first 2 ns and has tentatively been assigned to molecular reorganization induced by the sudden change in the lumophores' dipole moment upon excitation. The remaining shift can be associated with an exciton thermalization process, due to exciton diffusion through the doped molecular structure. The observed phenomenon is general in nature and provides insight into exciton dynamics during the luminescence process. Such information is essential in tailoring optimal performance of organic devices.

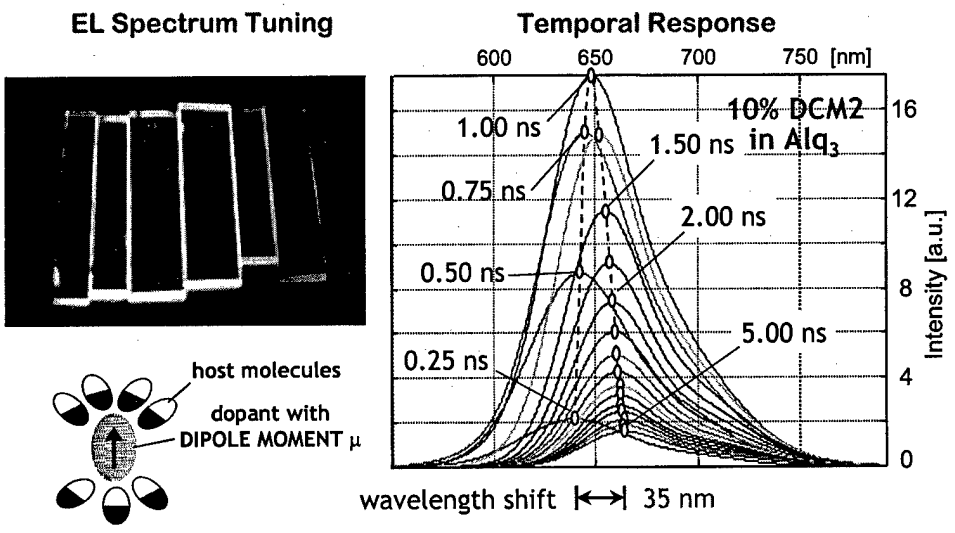

Figure 13 - Examples of temporal and static Solid State Solvation Effect.